

Entanglement Purification with Double Selection

Keisuke Fujii and Katsuji Yamamoto

Department of Nuclear Engineering, Kyoto University, Kyoto 606-8501, Japan

(Dated: October 31, 2018)

We investigate efficient entanglement purification through double selection process. This method works with higher noise thresholds for the communication channels and local operations, and achieves higher fidelity of purified states. Furthermore it provides a yield comparable to the usual protocol with single selection. It is shown by general considerations that the double selection is optimal to remove the first-order errors, achieving the upper bound on the fidelity of purified states in the low noise regime. The double selection is also applied to purification of multi-partite entanglement such as two-colorable graph states.

PACS numbers: 03.67.Hk, 03.67.Pp, 03.67.-a

I. INTRODUCTION

Recently a number of protocols based on entanglement have been developed in quantum communication and computation. For example, quantum teleportation, superdense coding, quantum cryptography and quantum repeater employ bipartite entanglement [1, 2, 3, 4]. Cluster state computation, quantum error correction and multiparty cryptography utilize multi-partite entanglement [5, 6, 7]. The performance of these entanglement-based protocols highly depends on the fidelity of entangled states. That is, high fidelity entangled states are essential for secure communication and reliable computation. In this viewpoint, it is a very important task to prepare and share high fidelity entangled states.

A way to share high fidelity entangled states via noisy communication channels is known as entanglement purification [8, 9]. This protocol is proposed originally to share EPR states, and then extended for a large class of multi-partite entangled states, including the GHZ states, two-colorable graph states, stabilizer states and W states [10, 11, 12, 13, 14, 15]. In a bipartite situation with noisy channels and perfect local operations, we pre-purify initial states with a recurrence protocol, which gives a high threshold for the noise of the communication channel but a low yield of purified states. Then, a hashing protocol may be implemented to get pure entangled states with a nonzero yield. The hashing protocol, however, breaks down as soon as local operations become slightly imperfect. The entanglement purification in such a situation is first analyzed in the context of quantum repeater [4], where the usual recurrence protocol [8, 9] is applied with imperfect local operations. In this situation, the fidelity of purified states is limited, and noise thresholds are required for the local operations as well as the communication channels. This is the most distinct point from the case with perfect local operations. Thus, in order to realize entanglement-based protocols using practical devices, which inevitably have imperfections, we need to develop efficient purification methods, which work well even with noisy communication channels and imperfect local operations.

In this paper we investigate an efficient entanglement

purification protocol with more accurate post-selection through double verification process. This method with double selection enables us to achieve considerably high fidelity of purified states even with actual imperfection. Furthermore it works with higher noise thresholds for the communication channels and local operations compared with the single-selection scheme [8, 9]. It may be considered that the elaborate post-selection consumes more resources to decrease the yield of purification. However, this is not necessarily the case. The present method with double selection provides a yield comparable to the single-selection scheme, especially when higher fidelity states are required with noisier local operations. It is really shown that the double selection is optimal to remove the first-order errors, achieving the upper bound on the fidelity of purified states in the low noise regime. The double selection is also applied to purification of multi-partite entanglement such as two-colorable graph states. As an example, we numerically investigate the performance for a CSS code (Steane's 7-qubit code), and compare it with a multi-partite purification protocol with single selection [11]. As the double selection can achieve considerably high fidelity under noisy channels and operations, it is indeed profitable for quantum computation as well as quantum communication.

The rest of the paper is organized as follow. In Sec. II we investigate the double selection in the bipartite entanglement purification. The performance of the double-selection protocol is analyzed in detail and compared with the usual protocol with single selection. The optimality of the double selection is also discussed in the low noise regime. The double selection is then applied to the multi-partite entanglement purification in Sec. III, where as an example the purification of the Steane's 7-qubit code is numerically investigated. Sec. IV is devoted to conclusion.

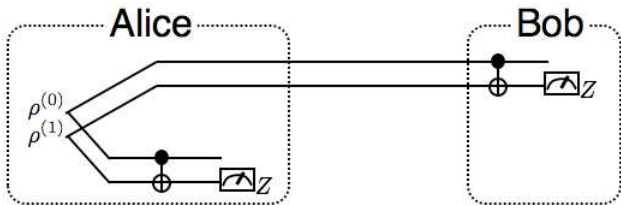


FIG. 1: Bipartite entanglement purification with single selection.

II. BIPARTITE ENTANGLEMENT PURIFICATION

A. Single selection

We first review the usual recurrence protocol for purification with single selection [8, 9]. Suppose Alice and Bob share EPR pairs, which are decohered via a noisy quantum channel, and purify them by using noisy C-Not gates and a classical channel. The recurrence protocol [8, 9] consists of two copies of an EPR pair, a bilateral C-Not gate and a bilateral measurement at each round of purification (see Fig. 1). Here, a bilateral operation means a tensor product of two identical operations which are simultaneously implemented by Alice and Bob. The purification procedure is specifically described as follows:

- (i) Alice and Bob share two identical EPR pairs $\rho^{(0)}$ and $\rho^{(1)}$ through a noisy quantum channel.
- (ii) They operate a bilateral C-Not gate for $\rho^{(0)}$ and $\rho^{(1)}$ as the control and target qubits, respectively.
- (iii) They bilaterally measure $\rho^{(1)}$ in the Z basis $\{|0\rangle, |1\rangle\}$, and obtain the measurement outcomes m_a (Alice) and m_b (Bob).
- (iv) They communicate these measurement outcomes to each other. Then, they keep $\rho^{(0)}$ if the measurement outcomes coincide as $m_a = m_b$. Otherwise, they discard $\rho^{(0)}$.

Alice and Bob iterate the procedures (ii)-(iv) by using the output states which survive the selection in (iv) as the input states for the next round of purification where the X and Z bases of their reference frames are exchanged with a Hadamard transformation [9]. As seen in the above, a single bilateral operation determines whether $\rho^{(0)}$ should be kept or discarded at each round. That is, the purification procedure is made with single selection.

The noisy EPR pairs $\rho^{(0)}$ and $\rho^{(1)}$ are given as two copies of a Bell diagonal state ρ ,

$$\rho^{(0)} = \rho^{(1)} = \rho = \sum_{j=0}^3 F_j \phi_j, \quad (1)$$

where

$$\phi_j = |\phi_j\rangle\langle\phi_j|, \quad (2)$$

$$|\phi_j\rangle = \sigma_j \otimes \sigma_0 (|00\rangle + |11\rangle) / \sqrt{2} \quad (3)$$

($\sigma_0 = I$). In the case with ideal (perfect) local operations, the above purification procedure with single selection provides the output states of $\rho^{(0)}$ depending on the initial states of $\rho^{(1)}$ as

$\rho^{(0)} \setminus \rho^{(1)}$	$\phi_0^{(1)}$	$\phi_1^{(1)}$	$\phi_2^{(1)}$	$\phi_3^{(1)}$
$\phi_0^{(0)}$	$\phi_0^{(0)}$	\times	\times	$\phi_3^{(0)}$
$\phi_1^{(0)}$	\times	$\phi_1^{(0)}$	$\phi_2^{(0)}$	\times
$\phi_2^{(0)}$	\times	$\phi_2^{(0)}$	$\phi_2^{(0)}$	\times
$\phi_3^{(0)}$	$\phi_3^{(0)}$	\times	\times	$\phi_0^{(0)}$

where \times denotes the output states discarded by the post-selection. Alice and Bob are to distill $|\phi_0\rangle$ with the largest probability F_0 (with a suitable basis transformation if necessary). For the most likely input state $\phi_0^{(0)} \otimes \phi_0^{(1)}$ with the probability F_0^2 , the purification procedure gives the desired output state $\phi_0^{(0)}$. On the other hand, the input state $\phi_0^{(0)} \otimes \phi_3^{(1)}$ with the probability $F_0 F_3$ results in a wrong output state $\phi_3^{(0)}$, and so on. This may be viewed as the σ_3 error of $\phi_3^{(1)} = (\sigma_3 \otimes \sigma_0) \phi_0^{(1)} (\sigma_3 \otimes \sigma_0)$ in $\rho^{(1)}$ is propagated to $\rho^{(0)}$ through the purification procedure. In this way, the purification procedure provides a map $\rho \rightarrow \rho'$ for the Bell diagonal states. This is even the case when the Pauli noise is introduced for the local operations, which is described later. This purification map can be represented by a $R^4 \rightarrow R^4$ map \mathcal{S} from the input state-vector $\mathbf{F} = (F_0, F_1, F_2, F_3)$ to the output state-vector $\mathbf{F}' = (F'_0, F'_1, F'_2, F'_3)$ as

$$\mathbf{F}' = \mathcal{S}(\mathbf{F}), \quad (4)$$

or in terms of a transition probability tensor S_i^{jk} as

$$F'_i = \frac{1}{p_{\mathcal{S}}(\mathbf{F})} \sum_{j,k} S_i^{jk} F_j F_k, \quad (5)$$

where

$$p_{\mathcal{S}}(\mathbf{F}) = \sum_{ijk} S_i^{jk} F_j F_k \quad (6)$$

is the success probability responsible for the normalization $\sum_i F'_i = 1$. The transition probability tensor S_i^{jk} is given including the noise parameters for the local operations and the exchange of the reference frames at each round (see Appendix A for the detail). Then the maximum achievable fidelity of purified states is determined as an appropriate fixed point of the map \mathcal{S} .

B. Double selection

We now present the entanglement purification with double selection. The double-selection protocol consists

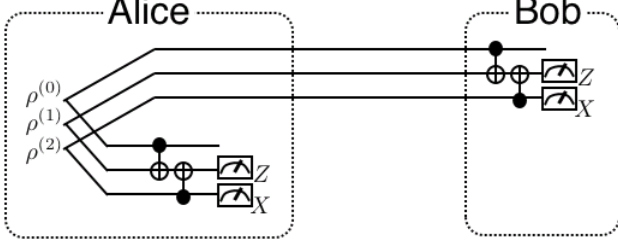


FIG. 2: Bipartite entanglement purification with double selection.

of three copies of EPR pairs, two bilateral C-Not gates and two bilateral measurements at each round of purification (see Fig. 2), as described in the following:

- (i) Alice and Bob share three identical EPR pairs $\rho^{(0)}$, $\rho^{(1)}$ and $\rho^{(2)}$ through a noisy quantum channel.
- (ii) They operate a bilateral C-Not gate for $\rho^{(0)}$ and $\rho^{(1)}$ as the control and target qubits, respectively.
- (iii) Next they operate a bilateral C-Not gate for $\rho^{(2)}$ and $\rho^{(1)}$ as the control and target qubits, respectively.
- (iv) They bilaterally measure $\rho^{(1)}$ and $\rho^{(2)}$ in the Z and X bases respectively, and obtain the measurement outcomes $m_a^{(1)}$, $m_a^{(2)}$ (Alice) and $m_b^{(1)}$, $m_b^{(2)}$ (Bob).
- (v) They communicate these measurement outcomes to each other. Then, they keep $\rho^{(0)}$ if both of the measurement outcomes coincide as $m_a^{(1)} = m_b^{(1)}$ and $m_a^{(2)} = m_b^{(2)}$. Otherwise, they discard $\rho^{(0)}$.

Similarly to the single-selection protocol, Alice and Bob iterate the procedures (ii)-(v) by using the output states which survive the selection in (v) as the input states for the next round where the X and Z bases of their reference frames are exchanged with a Hadamard transformation.

The action of these procedures with ideal local operations is described as

$\rho^{(0)} \setminus \rho^{(1)}$	$\phi_0^{(1)}$	$\phi_1^{(1)}$	$\phi_2^{(1)}$	$\phi_3^{(1)}$
$\phi_0^{(0)}$	$\phi_0^{(0)}$	\times	\times	\times
$\phi_1^{(0)}$	\times	$\phi_1^{(0)}$	\times	\times
$\phi_2^{(0)}$	\times	$\phi_2^{(0)}$	\times	\times
$\phi_3^{(0)}$	$\phi_3^{(0)}$	\times	\times	\times

with $\rho^{(2)} = \phi_0^{(2)}$, and so on with $\rho^{(2)} = \phi_1^{(2)}, \phi_2^{(2)}, \phi_3^{(2)}$. The double selection removes the errors more efficiently by using two ancilla EPR pairs. For example, as seen in the above table for $\phi_0^{(0)} \otimes \phi_3^{(1)}$ with $\phi_0^{(2)}$, we can detect and discard the Z error propagation as $\phi_0^{(0)} \otimes \phi_3^{(1)} \rightarrow \phi_3^{(0)}$ which is the first-order failure event in the single-selection scheme. Thus, this double selection process significantly

improves the maximum achievable fidelity of purified states. The optimality of the double selection to detect the first-order errors will be discussed in detail later.

The purification map \mathcal{D} of the double selection is described as

$$\mathbf{F}' = \mathcal{D}(\mathbf{F}), \quad (7)$$

or in terms of a transition probability tensor D_i^{jkl} as

$$F'_i = \frac{1}{p_{\mathcal{D}}(\mathbf{F})} \sum_{jkl} D_i^{jkl} F_j F_k F_l, \quad (8)$$

where

$$p_{\mathcal{D}}(\mathbf{F}) = \sum_{ijkl} D_i^{jkl} F_j F_k F_l \quad (9)$$

is the success probability responsible for the normalization. The transition probability tensor D_i^{jkl} is given in Appendix A.

C. Performance analysis and comparison

For each scheme, we investigate the performance by considering the working range of the local operations, the maximum achievable fidelity of purified states, the minimum fidelity required for the quantum communication channels and the EPR resources consumed to achieve a target fidelity. Here we assume that the imperfect C-Not gate is implemented as a perfect C-Not gate followed by two-qubit depolarizing errors with probabilities p_{ij} :

$$\mathcal{N}(\rho) = (1 - p_g)\rho + \sum_{(i,j)/(0,0)} p_{ij}(\sigma_i \otimes \sigma_j)\rho(\sigma_i \otimes \sigma_j), \quad (10)$$

where $i, j = 0, 1, 2, 3$, and $p_g = \sum_{(i,j)/(0,0)} p_{ij}$. The imperfect measurement in the Z basis is described with POVM elements and error probability p_m as

$$E_0 = (1 - p_m)|0\rangle\langle 0| + p_m|1\rangle\langle 1|, \quad (11)$$

$$E_1 = (1 - p_m)|1\rangle\langle 1| + p_m|0\rangle\langle 0|. \quad (12)$$

The imperfect measurement in the X basis is described similarly as

$$E_+ = H E_0 H, \quad (13)$$

$$E_- = H E_1 H, \quad (14)$$

where H denotes a Hadamard operation. Then the transition probability tensors S_i^{jk} and D_i^{jkl} , which characterize the purification maps \mathcal{S} and \mathcal{D} respectively, are calculated including the error probabilities p_{ij} and p_m (see Appendix A). By operating the purification map \mathcal{A} recursively, we can calculate the state-vector $\mathbf{F}^{(n)}$ at the n round of purification iteration as

$$\mathbf{F}^{(n)} = \mathcal{A}(\mathbf{F}^{(n-1)}) \quad (15)$$

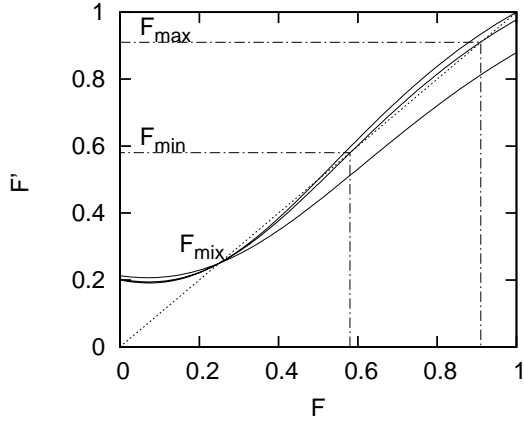


FIG. 3: Purification curve. The fidelity of the output state F' is plotted as a function of the fidelity of the input state F . Curves from top to bottom correspond to perfect local operations, imperfect local operations inside the working range, and those outside the working range.

($\mathcal{A} = \mathcal{S}$ for the single selection and \mathcal{D} for the double selection). The EPR states are shared initially through the noisy communication channel \mathcal{C} as

$$\mathcal{C}(\rho) = F_{\text{ch}}\rho + \frac{1 - F_{\text{ch}}}{3} \sum_{i=1}^3 \sigma_i \otimes \sigma_0 \rho \sigma_i \otimes \sigma_0. \quad (16)$$

Thus we set the initial state-vector for $\mathcal{C}(\phi_0)$ as

$$\mathbf{F}^{(0)} = \left(F_{\text{ch}}, \frac{1 - F_{\text{ch}}}{3}, \frac{1 - F_{\text{ch}}}{3}, \frac{1 - F_{\text{ch}}}{3} \right). \quad (17)$$

In the case with ideal local operations, the purification map \mathcal{A} has three fixed points for $F \equiv F_0$ and $F' \equiv F'_0$, i.e., the maximum achievable fidelity $F_{\text{max}} = 1$, the minimum required channel fidelity $F_{\text{min}} = 1/2$ and the completely mixed state $F_{\text{mix}} = 1/4$, as seen from the purification curve in Fig. 3. Then the imperfection of the local operations shifts down the purification curve. If the error probabilities p_g and p_m are inside the working range of the purification scheme, there still exist the three fixed points $F_{\text{max}} < 1$, $F_{\text{min}} > 1/2$ and $F_{\text{mix}} = 1/4$. In this case, if the communication channel has a fidelity F_{ch} higher than F_{min} , we can achieve the fidelity F_{max} by iterating the purification procedure. On the other hand, outside the working range, the purification procedure converts the noisy EPR state to the completely mixed state ($F_{\text{mix}} = 1/4$) with no entanglement.

The working range (p_g, p_m) of the local operations is shown in Fig. 4 for each purification scheme. Here the error probabilities of the C-Not gate are taken equally as $p_{ij} = p_g/15$. As seen in Fig. 4, the double-selection scheme has higher thresholds for the error probabilities than the single-selection scheme. Thus it works well with noisier local operations. If we choose a different error distribution $p_{i0} = p_{0i} = q_i$, $p_{ij} = q_i q_j$ ($i \neq j$ and $i, j \neq 0$)

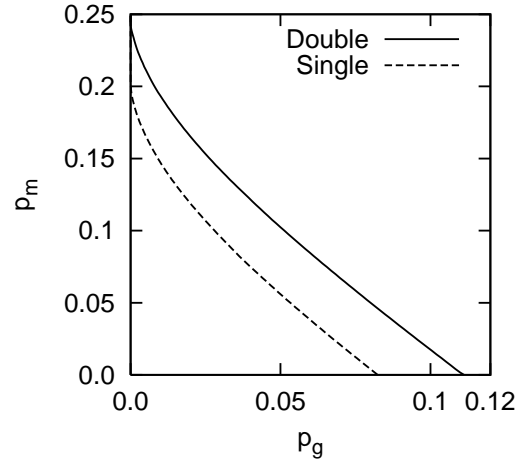


FIG. 4: Working range (p_g, p_m) of local operations. Each purification map \mathcal{A} has the non-trivial fixed points F_{max} and F_{min} for the error probabilities (p_g, p_m) below the threshold curve (solid line for \mathcal{D} and dotted line for \mathcal{S}).

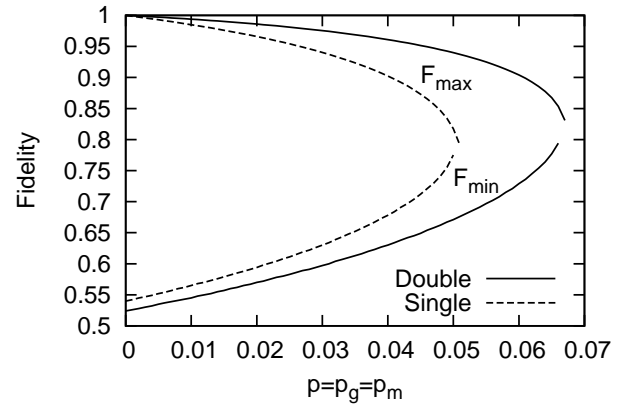


FIG. 5: Maximum achievable fidelity F_{max} (upper curves) and minimum required channel fidelity F_{min} (lower curves) are plotted as functions of the error probability $p = p_g = p_m$ for the double and single selections.

and $p_g = \sum_{i=1}^3 q_i$, as adopted in Ref. [16], we estimate the threshold values 3 – 4% and 4 – 5% of p_g with $p_m = 0$ for the single and double selections, respectively, which are consistent with an upper bound 5.3% derived in Ref. [16].

In Fig. 5, F_{max} (upper curves) and F_{min} (lower curves) are plotted as functions of the error probability p ($p = p_g = p_m$ for definiteness). The double selection achieves a higher fidelity of purification F_{max} with a less fidelity of communication channel F_{min} , compared with the single selection. These improvements are due to the fact that the double selection can detect more efficiently the first-

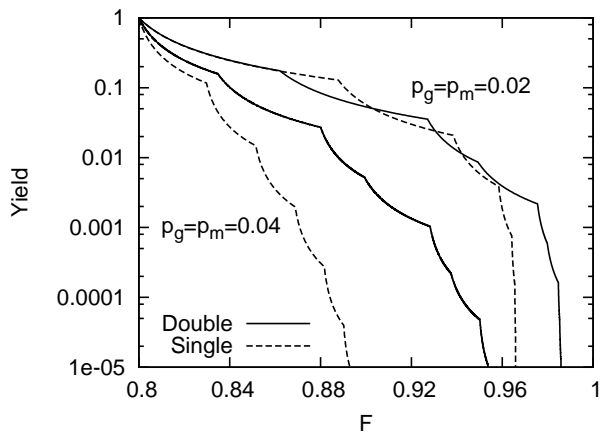


FIG. 6: The yield $Y_{\mathcal{A}}(F, F_{\text{ch}} = 0.8)$ is plotted as a function of the target fidelity F for each protocol with $p_g = p_m = 0.02$ (upper curves) and $p_g = p_m = 0.04$ (lower curves).

order errors, as discussed in detail later.

We compare the yields of the purification protocols. The yield $Y_{\mathcal{A}}(F, F_{\text{ch}})$ is defined as the inverse of the number of EPR pairs consumed to achieve a target fidelity F under the channel fidelity F_{ch} [15]. It is calculated for each scheme $\mathcal{A} = \mathcal{S}, \mathcal{D}$ as

$$Y_{\mathcal{A}}(F, F_{\text{ch}}) = \left[\prod_{n=1}^{n_{\mathcal{A}}(F, F_{\text{ch}})} N_{\mathcal{A}}/p_{\mathcal{A}}(\mathbf{F}^{(n-1)}) \right]^{-1}, \quad (18)$$

where $n_{\mathcal{A}}(F, F_{\text{ch}})$ denotes the minimum number of rounds which is required to achieve the fidelity F , $p_{\mathcal{A}}(\mathbf{F}^{(n-1)})$ denotes the probability to pass the purification procedure at the round n , as given in Eqs. (6) and (9), and $N_{\mathcal{A}}$ denotes the number of EPR pairs consumed at each round ($N_{\mathcal{S}} = 2$ and $N_{\mathcal{D}} = 3$). We plot in Fig. 6 the yield $Y_{\mathcal{A}}(F, F_{\text{ch}} = 0.8)$ as a function of the target fidelity F for each protocol with $p_g = p_m = 0.02$ (upper curves) and $p_g = p_m = 0.04$ (lower curves). With less noisy local operations ($p_g = p_m = 0.02$), both schemes provide comparable yields to achieve a target fidelity $F \approx 0.9$, where the numbers of rounds are $n_{\mathcal{S}} = 4$ (single) and $n_{\mathcal{D}} = 2$ (double). On the other hand, even when noisier local operations ($p_g = p_m = 0.04$) are used, the double-selection scheme still provides a reasonable yield to achieve a target fidelity $F \approx 0.9$, where $n_{\mathcal{S}} = 16$ and $n_{\mathcal{D}} = 4$. Since the double-selection scheme uses three EPR pairs at each round, it may be thought to cost more resources than the single-selection scheme with two EPR pairs at each round. However, this is not the case. As shown in the above, the double-selection scheme provides a comparable or even better yield. This is because the double-selection scheme increases the fidelity of EPR pairs considerably faster than the single-selection scheme. In the case of the double selection, an additional EPR pair is worth enough to enhance the fidelity of purified states, as discussed in the following.

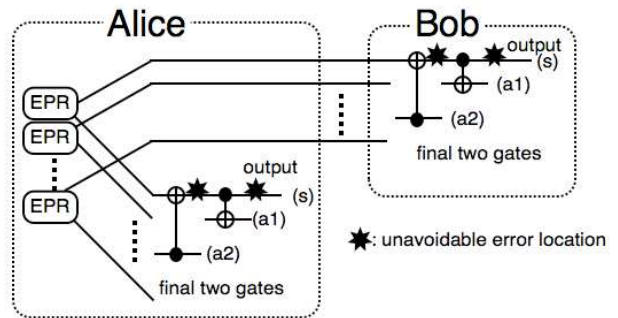


FIG. 7: Setup of a purification protocol. An upper bound on the fidelity is determined in the first order by the unavoidable errors (indicated by black stars) introduced by the final two C-Not gates. Similar bounds are obtained with other configurations of two-qubit gates.

D. Optimality of the double selection

We here discuss the optimality of the double selection in the first order of the errors. We first consider an upper bound on the fidelity of purified states by general arguments. Then, it will be shown that the double selection really saturates this upper bound in the low noise regime.

While purification protocols contain many imperfect local operations, we can reasonably derive an upper bound on the fidelity in the first order by noting the errors introduced by the final two gate operations applied on the source EPR pair. Here we assume that the local operations for purification are implemented by bilateral two-qubit Clifford gates and measurements. (One-qubit gates may be absorbed into relevant two-qubit gates and local reference frames.) Specifically, consider a purification protocol with a combination of two bilateral C-Not gates at the final step, as shown in Fig. 7. We inspect these final C-Not gate operations in the Alice's site to observe the undetectable errors left on the output state of the source qubit (s). (The same argument is made in the Bob's site.) Passing through this set of the final gates, the preceding errors on the source qubit (s) are propagated to either or both of the ancilla qubits (a1) and (a2). Thus these preceding errors are all regarded to be detectable, that is an optimal purification protocol is expected to remove them by post-selection after the measurements of the ancillas. The upper bound on the fidelity is rather determined by some of the errors introduced by the final two gates themselves (black stars in Fig. 7) which are undetectable and thus unavoidable without leaving any information on the ancillas. As for the second final C-Not gate, only the $\sigma_3^{(s)} \otimes \sigma_0^{(a2)}$ error with the probability p_{30} is undetectable, since it commutes with the final C-Not gate. On the other hand, all the $\sigma_i^{(s)} \otimes \sigma_0^{(a1)}$ errors of the final C-Not gate with the probabilities p_{i0} are undetectable inevitably, since the output source qubit does not interact with ancillas afterward. By adding these un-

detectable errors due to the final two C-Not gates in the sites of Alice and Bob, the upper bound on the fidelity is placed in the first order of the errors as

$$F_{\text{upper}} = 1 - 2 \left(p_{30} + \sum_{i=1}^3 p_{i0} \right) - \mathcal{O}(p_g^2). \quad (19)$$

Note here that the measurement error is not involved in considering the detectability of the errors with their propagation to the ancilla qubits. A portion of the right output state ϕ_0 may be discarded by the errors in measuring the ancillas for verification. This slight reduction of the right state is cancelled by the renormalization after the post-selection except for the higher-order contributions. Thus the measurement error does not contribute to the upper bound in the first order. The precise upper bound will be lower than this first-order bound due to the higher-order contributions of the gate and measurement errors, though it is beyond our scope to estimate them analytically.

Another protocol may be considered by exchanging the final two C-Not gates in Fig. 7. (This is actually the case in the recurrence protocol considered so far when the purification procedure is finished at an even round.) Similarly, by observing the undetectable errors introduced by the final two C-Not gates, the upper bound on the fidelity is placed as

$$F'_{\text{upper}} = 1 - 2 \left(p_{10} + \sum_{i=1}^3 p_{i0} \right) - \mathcal{O}(p_g^2). \quad (20)$$

We note that these upper bounds in Eqs. (19) and (20) are valid even if the final two C-Not gates are set in the same direction (e.g., both the C-Not gates are controlled by the source qubit). In such configurations, some of the preceding errors on the source qubit become undetectable, commuting with the final two gates. Thus these configurations merely lower the fidelity.

These two upper bounds F_{upper} and F'_{upper} coincide with each other for the uniform distribution of the gate errors $p_{ij} = p_g/15$, as adopted in calculating the maximum achievable fidelities of the single and double selections (Fig. 5). In general, the upper bound is given by $\max[F_{\text{upper}}, F'_{\text{upper}}]$ depending on the error distribution; in a recurrence protocol we should determine whether the purification procedure is finished at an even or odd round. We may also use other two-qubit Clifford gates instead of C-Not gates. Then, we obtain a similar upper bound with a suitable permutation among p_{i0} 's in Eq. (19) or Eq. (20), by considering which error of the second final gate is left commuting with the final gate.

We now show that the double selection really removes all the detectable errors in the first order, achieving the upper bound F_{upper} . (We here adopt the uniform error distribution for definiteness.) The recurrence protocol considered so far, with either single or double selection, has the setup as shown in Fig. 7 with the proper exchange of the reference frames at each round. In the

single selection (Fig. 1), the σ_1 and σ_2 (σ_2 and σ_3) errors on each ancilla EPR pair are detected by the Z (X) measurement, while the σ_3 (σ_1) error is not detected. In the double selection (Fig. 2), the primary ancilla EPR pair is further verified with the secondary ancilla EPR pair so that all the errors on the primary ancilla EPR pair are detected in the first order. That is, all the detectable errors on the source EPR pair are certainly removed by the double selection through the interaction with the primary ancilla EPR pairs, as expected in deriving the upper bound. Therefore, the double-selection protocol achieves the upper bound in the first order as

$$F_{\text{max}}^{\mathcal{D}} = F_{\text{upper}} - \mathcal{O}(p_g^2). \quad (21)$$

This has been really confirmed by the numerical calculation in the low gate noise regime $p_g < 0.02$, almost independently of the measurement error $p_m < 0.05$.

On the other hand, as noted above, in the single selection (Fig. 1) the σ_3 (σ_1) error on the ancilla EPR pair cannot be detected by the Z (X) measurement at an odd (even) round. Even in this case, all the errors before the second final C-Not gate are detected in the first order through the final two rounds, because the reference frames are properly exchanged at each round. However, some of the errors which have been excluded as detectable in deriving F_{upper} are actually left in the single-selection protocol. By counting these extra errors due to the final two C-Not gates in Fig. 7, we find that the maximum achievable fidelity of the single selection decreases as

$$F_{\text{max}}^{\mathcal{S}} = F_{\text{max}}^{\mathcal{D}} - (8/15)p_g - \mathcal{O}(p_g^2). \quad (22)$$

As seen so far, the double selection is necessary and sufficient to remove fully the detectable first-order errors, saturating the upper bound on the fidelity in the low noise regime. There is no room for the triple (or more) selection to improve the fidelity except for the higher-order error contributions. In practice, as the triple selection itself introduces more errors with additional noisy operations, it will hardly improve the maximum achievable fidelity of the double selection.

III. MULTI-PARTITE ENTANGLEMENT PURIFICATION

Recently entanglement purification is applied to a large class of multi-partite entanglements including two-colorable graph states [11, 13, 14]. We can extend the double-selection scheme to such protocols for multi-partite entanglement purification. Specifically, we here consider the purification of two-colorable graph states [11].

A graph state is expressed as an eigenstate of a set of stabilizer operators

$$K_j = X_j \bigotimes_{k \in V_j} Z_k, \quad (23)$$

where X_j and Z_k denote the Pauli operators acting on the j -th and k -th qubits respectively, and V_j denotes the set of vertices which are connected to the j -th qubit [17]. Then a graph state is described as

$$K_j |\Psi_{\mu_1 \mu_2 \dots \mu_N}\rangle = (-1)^{\mu_j} |\Psi_{\mu_1 \mu_2 \dots \mu_N}\rangle, \quad (24)$$

where $(-1)^{\mu_j}$ ($\mu_j = 0, 1$) denotes the eigenvalue ± 1 of the operator K_j . Especially a graph state which can be divided into two partitions A and B such that no vertices within one set are connected by edges is called a two-colorable graph state. It is described as

$$|\Psi_{\mu_A, \mu_B}\rangle, \quad (25)$$

where μ_A and μ_B denote the eigenvalues of the vertices within the partitions A and B , respectively.

The entanglement purification protocol with double selection for a noisy mixture of n -partite two-colorable graph states

$$\rho = \sum_{\mu_A, \mu_B} \lambda_{\mu_A, \mu_B} |\Psi_{\mu_A, \mu_B}\rangle \langle \Psi_{\mu_A, \mu_B}| \quad (26)$$

is implemented as follows (see Fig. 8):

- (i) Alice, Bob, \dots , Nancy share three identical two-colorable graph states $\rho^{(0)}$, $\rho^{(1)}$ and $\rho^{(2)}$ through a noisy quantum channel.
- (ii) They operate a multi-lateral C-Not gate for $\rho^{(0)}$ and $\rho^{(1)}$ with the partition A [B] of $\rho^{(0)}$ [$\rho^{(1)}$] as the control and the partition A [B] of $\rho^{(1)}$ [$\rho^{(0)}$] as the target, respectively.
- (iii) Similarly they operate a multi-lateral C-Not gate for $\rho^{(2)}$ and $\rho^{(1)}$.
- (iv) They multi-laterally measure the partition A [B] of $\rho^{(1)}$ and the partition A [B] of $\rho^{(2)}$ in the Z and X [X and Z] bases respectively, and obtain measurement outcomes $(-1)^{\xi_i^{(1)}} [(-1)^{\zeta_j^{(1)}}]$ and $(-1)^{\xi_i^{(2)}} [(-1)^{\zeta_j^{(2)}}]$, where $\xi_i, \zeta_j = 0, 1$, and the qubit i [j] belongs to the partition A [B].
- (v) They communicate these measurement outcomes to each other. Then they keep $\rho^{(0)}$ if for all i and j , $\zeta_j^{(1)} \oplus \sum_{k \in V_j} \xi_k^{(1)} = 0$ and $\xi_i^{(2)} \oplus \sum_{k \in V_i} \zeta_k^{(2)} = 0$, which implies $\mu_A^{(0)} \oplus \mu_A^{(1)} \oplus \mu_A^{(2)} = \mathbf{0}$ and $\mu_B^{(1)} \oplus \mu_B^{(2)} = \mathbf{0}$, respectively, where \oplus denotes bitwise addition modulo 2.

They iterate the procedures (ii)-(v) by using the output states which survive the selection in (v) as the input states for the next round where the X and Z bases of their reference frames are exchanged with a Hadamard transformation, similarly to the bipartite case. These

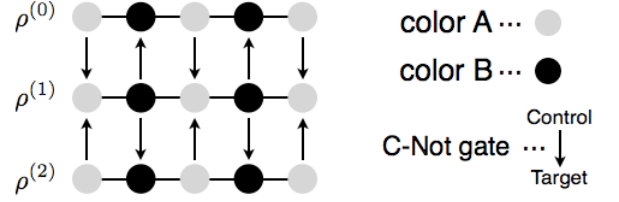


FIG. 8: Purification of two-colorable graph states with double selection.

procedures with perfect operations act as

$$|\Psi_{\mu_A^{(0)}, \mu_B^{(0)}}^{(0)}\rangle \rightarrow |\Psi_{\mu_A^{(0)}, \mu_B^{(0)} \oplus \mu_B^{(1)}}^{(0)}\rangle, \quad (27)$$

$$|\Psi_{\mu_A^{(1)}, \mu_B^{(1)}}^{(1)}\rangle \rightarrow |\Psi_{\mu_A^{(0)} \oplus \mu_A^{(1)} \oplus \mu_A^{(2)}, \mu_B^{(1)}}^{(1)}\rangle, \quad (28)$$

$$|\Psi_{\mu_A^{(2)}, \mu_B^{(2)}}^{(2)}\rangle \rightarrow |\Psi_{\mu_A^{(2)}, \mu_B^{(1)} \oplus \mu_B^{(2)}}^{(2)}\rangle. \quad (29)$$

Thus in the double-selection scheme we can detect even the propagation of the errors $\mu_B^{(1)}$ from $\rho^{(1)}$ to $\rho^{(0)}$ by using $\rho^{(2)}$ the same as the bipartite case.

As an example of the multi-partite purification with the double selection, we numerically investigate a CSS code state, specifically the Steane's 7-qubit code state, which is a two-colorable graph state. Then its performance is compared with the ADB protocol [11]. We consider the multiparty communication situation, where n -qubit two-colorable graph states $|\Psi_{\mathbf{0}_A, \mathbf{0}_B}\rangle \langle \Psi_{\mathbf{0}_A, \mathbf{0}_B}|$ are shared through n identical noisy channels $\mathcal{C}^{\otimes n}$. The noisy copies $\rho_{\text{in}} = \mathcal{C}^{\otimes n}(|\Psi_{\mathbf{0}_A, \mathbf{0}_B}\rangle \langle \Psi_{\mathbf{0}_A, \mathbf{0}_B}|)$ of the n -qubit entangled state are purified with the noisy C-Not gates and measurements the same as the bipartite case. We simulate directly the noisy operations in the communication and purification procedures by using Monte-Carlo method. (It is highly complicated to provide the purification map in terms of the transition probability tensor.) The fidelity of the purified state ρ' is measured by

$$F(\rho', |\Psi_{\mathbf{0}_A, \mathbf{0}_B}\rangle) = \langle \Psi_{\mathbf{0}_A, \mathbf{0}_B} | \rho' | \Psi_{\mathbf{0}_A, \mathbf{0}_B} \rangle. \quad (30)$$

If the initial fidelity

$$F_{\text{in}} \equiv F(\rho_{\text{in}}, |\Psi_{\mathbf{0}_A, \mathbf{0}_B}\rangle) = F_{\text{ch}}^7 + \mathcal{O}((1 - F_{\text{ch}})^3) \quad (31)$$

is higher than F_{min} , we can achieve the fidelity F_{max} by iterating the purification procedure.

The resultant maximum achievable fidelity F_{max} and minimum required initial fidelity F_{min} are plotted for the Steane's 7-qubit code state $|\Psi_{\mathbf{0}_A, \mathbf{0}_B}\rangle = |0_L\rangle$ as functions of the error probability $p = p_g = p_m$ in Fig. 9. As we expect, the double-selection protocol achieves considerably higher fidelity of the purified states requiring lower fidelity of the channels. Then the noise threshold for the local operations is improved from 5–6% (single) to 8–9% (double). It is also seen in Fig. 10 that both schemes provide comparable yields, similarly to the bipartite case.

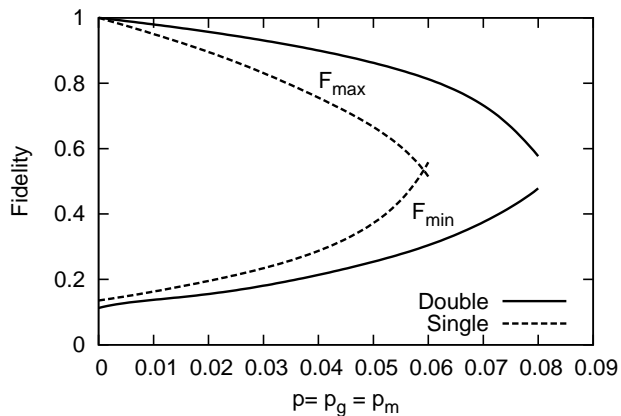


FIG. 9: Maximum achievable fidelity F_{\max} (upper curves) and minimum required channel fidelity F_{\min} (lower curves) for the Steane's 7-qubit code state $|0_L\rangle$ are plotted as functions of the error probability $p = p_g = p_m$ for the single and double selections.

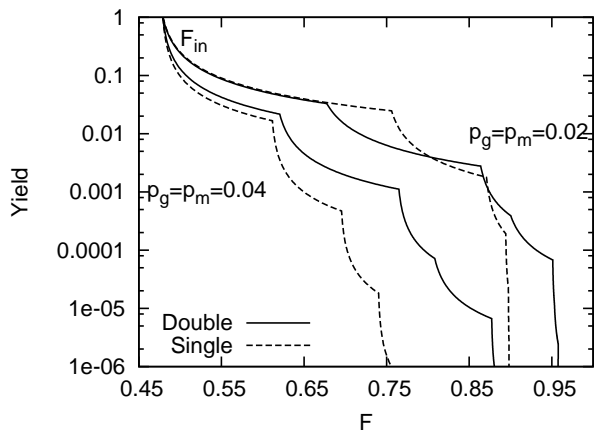


FIG. 10: The yield $Y_A(F, F_{\text{ch}} = 0.9)$ is plotted as a function of the target fidelity F for each protocol with $p_g = p_m = 0.02$ (upper curves) and $p_g = p_m = 0.04$ (lower curves).

The yields are, however, significantly low compared with the bipartite case. This is because the coincidence of the more measurement outcomes is required in the multipartite case, reducing the success probability of post-selection. The upper bound on the fidelity with imperfect local operations can be extended to the two-colorable graph states in the same line. Then the maximum achievable fidelity F_{\max} of the double-selection scheme saturates the upper bound $F_{\text{upper}} = 1 - 7 \times (4/15)p_g$ for $n = 7$ with $p_{ij} = p_g/15$, which is really confirmed in the low noise regime by the numerical simulation.

The two-colorable graph states, including cluster and CSS code states, play very important roles in quantum computation as well as quantum communication. Then these results really indicate that the double selection is

profitable also in quantum computation. In fact, encoded ancilla qubits are used to stabilize a computation in a fault-tolerant way, and the performance of computation highly depends on the fidelity of these ancilla qubits [18, 19]. In the usual fault-tolerant context [19, 20, 21], these encoded ancilla qubits are prepared through the single selection. Thus the double selection has a good potential to improve the noise threshold of fault-tolerant computation. The verification process with the double selection is used in fault-tolerant computation with concatenated construction of verified logical cluster states, achieving a considerably high noise threshold $\sim 4\%$ [22]. We will discuss elsewhere further applications of the double selection for quantum computation.

IV. CONCLUSION

We have investigated entanglement purification with double selection. It has been shown that the maximum achievable fidelity can be improved significantly by the double selection under noisy communication channels and imperfect local operations. Furthermore the double-selection scheme provides a reasonable yield, which is comparable or even better than the single-selection scheme. The double selection is really optimal to remove the first-order errors, achieving the upper bound on the fidelity of purified states in the lower noise regime. These results really indicate that the double selection is more suitable for realization of entanglement-based protocols. The double selection is also applied to multi-partite entanglement purification, specifically two-colorable graph states. The improvement of the fidelity has been shown numerically for the Steane's 7-qubit code state. The double selection can be extended to all graph states in the same way. Since multi-partite entangled states, such as CSS codes and cluster states, play very important roles in quantum computation as well as quantum communication, the double selection has a good potential to improve the performance of quantum computation.

Acknowledgments

This work was supported by JSPS Research Fellowships for Young Scientists No. 20-2157.

APPENDIX A: DERIVATION OF TRANSITION PROBABILITY TENSORS

The purification procedure of the single selection before the post-selection is described as a linear map \tilde{S} of the two Bell states $\phi_i^{(0)}$ and $\phi_j^{(1)}$ as

$$\tilde{S}(\phi_i^{(0)} \otimes \phi_j^{(1)}) = \tilde{S}_{kl}^{ij} \phi_k^{(0)} \otimes \phi_l^{(1)}. \quad (\text{A1})$$

This map consists of the noisy bilateral C-Not gate $\mathcal{G}(\phi_i^{(0)} \otimes \phi_j^{(1)}) = G_{ab}^{ij} \phi_a^{(0)} \otimes \phi_b^{(1)}$, the bilateral Z -basis measurement with error $\mathcal{M}(\phi_b^{(1)}) = M_l^b \phi_l^{(1)}$ and the exchange of the reference frames at each round by the bilateral H transformation (ideal for simplicity) $\mathcal{H}(\phi_a^{(0)}) = H_k^a \phi_k^{(0)}$:

$$\tilde{S}_{kl}^{ij} = H_k^a M_l^b G_{ab}^{ij}. \quad (\text{A2})$$

The noisy bilateral C-Not gate G_{km}^{ij} is decomposed into the ideal bilateral C-Not gate U_{ab}^{ij} and the bilateral combination $N_{km}^{cd} N_{cd}^{ab}$ of the C-Not gate noises at Alice and Bob:

$$G_{km}^{ij} = N_{km}^{cd} N_{cd}^{ab} U_{ab}^{ij}. \quad (\text{A3})$$

Note here that the Bell states are two-colorable graph states up to a local Hadamard operation as

$$|\phi_i\rangle = (I \otimes H) |\Psi_{\mu_A^i, \mu_B^i}\rangle, \quad (\text{A4})$$

where

$$\boldsymbol{\mu}^i = (\mu_A^i, \mu_B^i) = (0, 0), (1, 0), (1, 1), (0, 1) \quad (\text{A5})$$

for $i = 0, 1, 2, 3$, respectively. In the graph state representation, the action of the ideal bilateral C-Not gate is described as

$$|\Psi_{\mu_A^i, \mu_B^i}^{(0)}\rangle |\Psi_{\mu_A^j, \mu_B^j}^{(1)}\rangle \rightarrow |\Psi_{\mu_A^i, \mu_B^i \oplus \mu_B^j}^{(0)}\rangle |\Psi_{\mu_A^i \oplus \mu_A^j, \mu_B^j}^{(1)}\rangle, \quad (\text{A6})$$

or simply

$$\tilde{\mathcal{U}}(\boldsymbol{\mu}^i \otimes \boldsymbol{\mu}^j) = (\mu_A^i, \mu_B^i \oplus \mu_B^j) \otimes (\mu_A^i \oplus \mu_A^j, \mu_B^j). \quad (\text{A7})$$

Then the transition tensor of the ideal bilateral C-Not gate is given by

$$U_{ab}^{ij} = \begin{cases} 1 & [\boldsymbol{\mu}^i \otimes \boldsymbol{\mu}^j = \tilde{\mathcal{U}}(\boldsymbol{\mu}^a \otimes \boldsymbol{\mu}^b)] \\ 0 & [\boldsymbol{\mu}^i \otimes \boldsymbol{\mu}^j \neq \tilde{\mathcal{U}}(\boldsymbol{\mu}^a \otimes \boldsymbol{\mu}^b)] \end{cases}, \quad (\text{A8})$$

e.g., $U_{22}^{13} = 1$ for $\boldsymbol{\mu}^2 \otimes \boldsymbol{\mu}^2 = (1, 1) \otimes (1, 1) \rightarrow (1, 0) \otimes (0, 1) = \boldsymbol{\mu}^1 \otimes \boldsymbol{\mu}^3$ by $\tilde{\mathcal{U}}$, and so on. The noise on the C-Not gate is given by

$$N_{cd}^{ab} = p_{ij} [(ac) \in \mathcal{P}_{\sigma_i}, (bd) \in \mathcal{P}_{\sigma_j}], \quad (\text{A9})$$

e.g., $N_{10}^{00} = p_{10}$ for $(ac) = (01)$ with $\sigma_1 \otimes \sigma_0 \phi_0 \sigma_1 \otimes \sigma_0 = \phi_1$ and $(bd) = (00)$ with $\sigma_0 \otimes \sigma_0 \phi_0 \sigma_0 \otimes \sigma_0 = \phi_0$, and so on, where $p_{00} = 1 - \sum_{(i,j)/(0,0)} p_{ij} = 1 - p_g$, and σ_i 's provide

the permutations among the Bell states ϕ_i 's as

$$\mathcal{P}_{\sigma_0} = \begin{pmatrix} 0 & 1 & 2 & 3 \\ 0 & 1 & 2 & 3 \end{pmatrix}, \quad (\text{A10})$$

$$\mathcal{P}_{\sigma_1} = \begin{pmatrix} 0 & 1 & 2 & 3 \\ 1 & 0 & 3 & 2 \end{pmatrix}, \quad (\text{A11})$$

$$\mathcal{P}_{\sigma_2} = \begin{pmatrix} 0 & 1 & 2 & 3 \\ 2 & 3 & 0 & 1 \end{pmatrix}, \quad (\text{A12})$$

$$\mathcal{P}_{\sigma_3} = \begin{pmatrix} 0 & 1 & 2 & 3 \\ 3 & 2 & 1 & 0 \end{pmatrix}. \quad (\text{A13})$$

The bilateral Z -basis measurement is given by

$$M_l^b = m_l^e m_e^b \quad (\text{A14})$$

as a product of the single measurements given by

$$m_e^b = \begin{cases} 1 - p_m & [(be) \in \mathcal{P}_{\sigma_0}] \\ p_m & [(be) \in \mathcal{P}_{\sigma_1}] \\ 0 & [(be) \in \mathcal{P}_{\sigma_2}, \mathcal{P}_{\sigma_3}] \end{cases}. \quad (\text{A15})$$

The bilateral Hadamard operation is given by

$$H_k^a = h_k^e h_e^a, \quad (\text{A16})$$

where $h_0^0 = h_3^1 = h_2^2 = h_1^3 = 1$ and $h_e^a = 0$ for the others. After all the transition probability tensor S_i^{jk} of the single selection is obtained by picking up the post-selected states with $l = 0, 3$ from \tilde{S}_{il}^{jk} as

$$S_i^{jk} = \tilde{S}_{i0}^{jk} + \tilde{S}_{i3}^{jk}. \quad (\text{A17})$$

Similarly, the purification procedure of the double selection before the post-selection is described as a linear map \tilde{D} of the three Bell states $\phi_i^{(0)}, \phi_j^{(1)}, \phi_k^{(2)}$ as

$$\tilde{D}_{lmn}^{ijk} = H_l^a M_m^c \tilde{M}_n^d G_{dc}^{kb} G_{ab}^{ij}, \quad (\text{A18})$$

where

$$\tilde{M}_n^d = H_n^f M_f^e H_e^d \quad (\text{A19})$$

provides the X -basis measurement. Then the transition probability tensor of the double selection is obtained by the post-selection as

$$D_i^{jkl} = \sum_{m=0,3;n=0,1} \tilde{D}_{imn}^{jkl}. \quad (\text{A20})$$

-
- [1] C. H. Bennett, G. Brassard, C. Crépeau, R. Jozsa, A. Peres, and W. K. Wootters, *Phys. Rev. Lett.* **70**, 1895 (1993).
- [2] C. H. Bennett and S. J. Wiesner, *Phys. Rev. Lett.* **69**, 2881 (1992).
- [3] A. K. Ekert, *Phys. Rev. Lett.* **67**, 661 (1991).
- [4] H.-J. Briegel, W. Dür, J. I. Cirac, and P. Zoller, *Phys. Rev. Lett.* **81**, 5932 (1998); W. Dür, H.-J. Briegel, J. I. Cirac, and P. Zoller, *Phys. Rev. A* **59**, 169 (1999).
- [5] R. Raussendorf and H.-J. Briegel, *Phys. Rev. Lett.* **86**, 5188 (2001); R. Raussendorf, D. E. Browne, and H.-J. Briegel, *Phys. Rev. A* **68**, 022312 (2003).
- [6] P. W. Shor, *Proceedings of the 37th Annual Symposium on Foundations of Computer Science* (IEEE Computer Society Press, Los Alamitos, CA, 1996), p. 56.
- [7] K. Chen and H.-K. Lo, *Quant. Inf. Comp.* **7**, 689 (2007).
- [8] C. H. Bennett, G. Brassard, S. Popescu, B. Schumacher, J. A. Smolin, and W. K. Wootters, *Phys. Rev. Lett.* **76**, 722 (1996); C. H. Bennett, D. P. DiVincenzo, J. A. Smolin, and W. K. Wootters, *Phys. Rev. A* **54**, 3824 (1996).
- [9] D. Deutsch, A. Ekert, R. Jozsa, C. Macchiavello, S. Popescu, and A. Sanpera, *Phys. Rev. Lett.* **77**, 2818 (1996).
- [10] M. Muraao, M. B. Plenio, S. Popescu, V. Vedral, and P. L. Knight, *Phys. Rev. A* **57**, R4075 (1998).
- [11] W. Dür, H. Aschauer, and H.-J. Briegel, *Phys. Rev. Lett.* **91**, 107903 (2003); H. Aschauer, W. Dür, and H.-J. Briegel, *Phys. Rev. A* **71**, 012319 (2005).
- [12] S. Glancy, E. Knill, and H. M. Vasconcelos, *Phys. Rev. A* **74**, 032319 (2006).
- [13] C. Kruszynska, A. Miyake, H.-J. Briegel, and W. Dür, *Phys. Rev. A* **74**, 052316 (2006).
- [14] A. Miyake and H.-J. Briegel, *Phys. Rev. Lett.* **95**, 220501 (2005).
- [15] C. Kruszynska, S. Anders, W. Dür, and H.-J. Briegel, *Phys. Rev. A* **73**, 062328 (2006).
- [16] A. Kay, *Phys. Rev. A* **77**, 052319 (2008).
- [17] W. Dür and H.-J. Briegel, *Rep. Prog. Phys.* **70**, 1381 (2007).
- [18] B. Eastin, *Phys. Rev. A* **75**, 022301 (2007).
- [19] E. Knill, *Nature* **434**, 39 (2005).
- [20] A. M. Steane, *Phys. Rev. Lett.* **78**, 2252 (1997).
- [21] A. W. Cross, D. P. DiVincenzo, and B. M. Terhal, arXiv:0711.1556 (2007).
- [22] K. Fujii and K. Yamamoto, arXiv:0802.4137 (2008).